THE JOURNAL OF PHYSICAL CHEMISTRY B

Article

pubs.acs.org/JPCB

Insights into the Catalytic Mechanism of Coral Allene Oxide Synthase: A Dispersion Corrected Density Functional Theory Study

Eric A. C. Bushnell, Rami Gherib, and James W. Gauld*

Department of Chemistry and Biochemistry, University of Windsor, Windsor, Ontario N9B 3P4, Canada

Supporting Information

ABSTRACT: In this present work the mechanism by which cAOS catalyzes the formation of allene oxide from its hydroperoxy substrate was computationally investigated by using a DFT-chemical cluster approach. In particular, the effects of dispersion interactions and DFT functional choice (M06, B3LYP, B3LYP*, and BP86), as well as the roles of multistate reactivity and the tyrosyl proximal ligand, were examined. It is observed that the computed relative free energies of stationary points along the overall pathway are sensitive to the choice of DFT functional, while the mechanism obtained is generally not. Large reductions in relative free energies for stationary points along the pathway (compared to the initial reactant complex) of on average 46.3 and 97.3 kJ mol^{-1} for the doublet and quartet states, respectively, are observed upon going from the M06 to BP86 functional. From results obtained by using the B3LYP* method, well-tested previously on heme-containing systems, the mechanism of cAOS appears to occur with considerably higher Gibbs free energies than that for the analogous pathway in pAOS, possibly due to the presence of a ligating tyrosyl residue in cAOS. Furthermore, at the IEFPCM-B3LYP*/6-311+G(2df,p)//B3LYP/BS1 level of theory the inclusion of dispersion effects leads to the suggestion that the overall mechanism of cAOS could occur *without* the need for spin inversion.

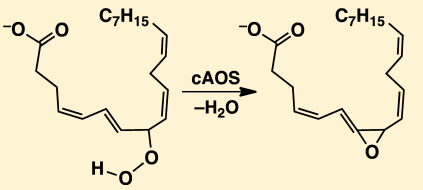

INTRODUCTION

Oxylipins are involved in numerous signaling and development processes in almost all living organisms.[1] A key enzyme in their synthesis is allene oxide synthase (AOS).[2] In plants this enzyme (pAOS) is a member of the CYP74A subfamily of the P450 family of hemoproteins with a cysteinyl residue as the heme's proximal ligand.[3] In contrast, in coral AOS (cAOS) the active site structure shows a remarkable resemblance to Catalase as it has a tyrosyl proximal ligand.[4] Regardless of these differences it has been proposed that both enzymes catalyze their reactions via similar chemistry.[3a]

The proposed mechanism (Scheme 1) for cAOS begins with the binding of 8(*R*)-hydroperoxyeicosatetraenoic (8(*R*)-HPETE) acid (**A**).[4a] Subsequently, homolytic cleavage of the O−O bond occurs generating an alkoxy radical and compound II (Cpd II) intermediate complex with an Fe-bound hydroxyl group (**B**). It is noted that an alternative form of Cpd II exists where the oxygen is doubly bound to the Fe center (i.e. deprotonated). Cyclization of the alkoxy radical results in formation of an epoxide allylic radical (**C**) that is then subsequently oxidized via electron transfer (ET) onto Cpd II.[4a] This results in the formation of a cationic center on the epoxide intermediate (**D**). The last step is proton transfer from the substrates C9 center to an active site histidyl (H67) residue to generate the C═C double bond adjacent to the epoxide moiety (**E**).[4a]

Recently the mechanism of pAOS was investigated by Cho et al.[5] using a QM/MM approach. More specifically, they used the density functional theory hybrid method B3LYP/LACVP (i.e. 6-31G on all atoms + LANL2DZ on Fe) and the CHARMM27 force field for the high and low layers, respectively. Notably, unlike that experimentally proposed,[6] they did not obtain an Fe-peroxy bound reactive complex for either the high spin (i.e. sextet; $S = {}^5/_2$) or low spin (i.e. doublet; $S = {}^1/_2$) state with the latter being the most favored.[5] Instead, they concluded that O−O homolytic bond cleavage of the peroxide substrate occurred concomitantly with substrate binding. Moreover, a spin inversion from the sextet state to the doublet state occurred as well.[5] This step was found to be rate limiting with the subsequent generation of the epoxide allylic radical occurring without a barrier. Due to the lack of an active site histidyl in pAOS, the last step, oxidation of the epoxide allylic radical, proceeded in one step via hydrogen atom transfer from the substrate to the oxo-ferryl species rather than in two separate steps as proposed for cAOS.[5] Unfortunately, as they only investigated the mechanism for the doublet state (with the exception of the sextet reactive complex), the possible role of multistate reactivity (MSR), a common feature in transition metal chemistry, was not considered.[7]

The interactions between substrates and proteins are commonly a combination of van der Waals (vdW), electrostatic, and hydrogen bonding interactions.[8] Indeed, it has been shown that inclusion of vdW effects is important for reliably computationally modeling the binding of small molecules to model heme systems.[9] However, the proper description of such dispersion interactions is a well-known limitation of commonly used DFT functionals such as B3LYP.[10] For instance, a number of computational studies have examined the effects of

Received: April 6, 2013
Revised: May 13, 2013

   dx.doi.org/10.1021/jp403405b | J. Phys. Chem. B XXXX, XXX, XXX−XXX

Scheme 1. The Proposed Catalytic Mechanism of cAOS (see ref 4a)[a]

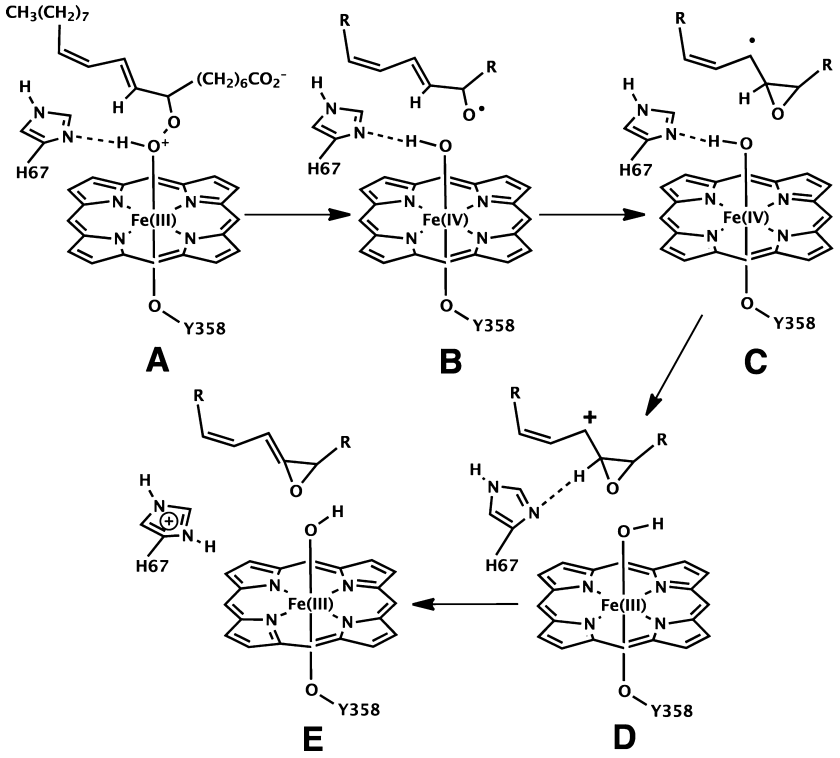

[a]For reasons of clarity not all hydrogens have been added while the porphyrin ring is shown as a porphine ring.

dispersion on the reactions of P450-enzymes using both small DFT-cluster and QM/MM approaches.[11] From the results obtained it was concluded that for the reactions considered the inclusion of dispersion effects lowered barriers considerably. Importantly, they were as a result in better agreement with experiment.[11b,c] Recently, Hirao[12] examined the performance of various DFT functionals with empirical dispersion corrections included to properly describe the Co−C bond dissociation energies of methyl cobalamin, a corrin ring containing molecule. It was found that good agreement with experiment[13] was only obtained upon inclusion of dispersion effects.[12] In addition, Hirao[14] examined O_2 binding by the nonheme iron enzyme *myo*-inositol oxygenase using a dispersion corrected QM/MM approach. Notably, they concluded that the reliable modeling of vdW interactions was important for properly describing the binding of O_2 within the active site.

In this current work the mechanism by which cAOS catalyzes the synthesis of allene oxide from its hydroperoxy substrate has been computationally investigated by using a DFT-chemical cluster approach. To the best of our knowledge it is the first such study on cAOS. In particular we have systematically examined the effect of dispersion interactions and multistate reactivity along the mechanism, the choice of DFT functional, and the role of the tyrosyl proximal ligand of cAOS compared to the cysteinyl found in pAOS.

COMPUTATIONAL METHODS

Molecular Docking. The Molecular Operating Environment (MOE)[15] software package was used to perform the molecular docking calculations. The crystal structure of the AOS-lipoxygenase protein from *P. homomalla* (PDB: 3DY5) was used as a template. Prior to docking, all crystallographic waters and counterions were removed as well as the C-terminal lipoxygenase domain. Experimentally it was shown that the catalytic activity of the N-terminal AOS domain was retained upon deletion of the C-terminal domain.[3a] The coordinates of hydrogens were then added by using the MOE default method. The substrate, modeled as 8*R*-hydroperoxyeicosatetraenoic acid (8(*R*)-HPETE) was then docked within the active site. The binding free energy of each enzyme−substrate complex generated by this procedure was estimated with the London dG scoring function. The geometries of the top one hundred complexes were then optimized by using the Forcefield refinement scheme in conjunction with the AMBER99 force field.[16] After minimization the binding free energies were recalculated with the London dG scoring function. The top scoring complex was then minimized by using the AMBER99 force field until the root-mean-square gradient of the total energy fell below 0.05 kcal au^{-1}. It is noted that in all top scoring conformers the substrates' peroxy moiety was ligated to the Fe center while its carboxy ($R\text{-}COO^-$) headgroup formed a salt bridge with K105.

QM Calculations. The Gaussian09 program suite was used to perform all DFT-cluster calculations.[17] This approach has been successfully widely used on related systems and reviewed in detail elsewhere.[18] The stationary points on the free energy surface (PES) were located at the B3LYP/BS1 level of theory.[19] The combination of basis functions defined by BS1 are the 6-31G basis set on all atoms except Fe and the peroxy oxygens. For Fe a combination of the 6-311+G(2df) basis set (for valence orbitals) and LANL2DZ ECP (for core orbitals) was used while the peroxy oxygens were described by the 6-31+G(d) basis set. It has been previously shown that diffuse functions are essential for a proper description of the O−O homolytic cleavage process in the formation of Cpd I.[20] Frequency analyses of all stationary points was done at the

dx.doi.org/10.1021/jp403405b | J. Phys. Chem. B XXXX, XXX, XXX−XXX

same level of theory in order to characterize them as minima or transition states as well as to obtain the corresponding Gibbs free-energy corrections (ΔG_{Cor}). Notably, B3LYP has been successfully used to investigate the mechanism and properties of catalase enzymes.[21] Importantly, as noted in the Introduction the active site structure of cAOS shows a remarkable resemblance to Catalase as it has a tyrosyl proximal ligand.[4]

Dispersion interactions, which are not well described in B3LYP, were corrected for via the use of single point calculations involving dispersion correcting potentials (DCP).[22] More specifically, single point calculations were performed at the B3LYP/6-31+G(d,p) level of theory on the above optimized geometries. These were then recalculated by using a modified 6-31+G(d,p) basis set in which two basis functions have been added on each carbon, as detailed in the work of DiLabio.[23] For each complex the difference in energies was taken as the dispersion correction ($\Delta Disp_{Cor}$). It is noted that the use of DCPs has been shown to provide more reliable reaction thermodynamics.[23b]

Reducing the amount of exact exchange in B3LYP to 15% (i.e. use of the B3LYP* method) has been shown to give relative energies in better agreement with experiment.[9] Moreover, it has been stated that the use of B3LYP* has been shown to be better when describing the oxidation of transition metal containing compounds providing an improvement over the standard B3LYP functional.[9,18a] Furthermore, as shown in a recent investigation of 8R-LOX, geometry optimizations are less sensitive to the amount of exact exchange in B3LYP; it was found that in general the energies are more sensitive.[24] Hence relative energies were determined via single point calculations at the IEFPCM-B3LYP*/6-311+G(2df,p)//B3LYP/BS1 level of theory and corrected by inclusion of ΔG_{Cor} and ΔD_{Cor}, unless otherwise noted.[25] The IEFPCM approach with a dielectric constant of 4.0 was used to model the polarizing effect of the protein environment.[18b,26]

The M06 functional has been suggested to provide a better account of dispersion interactions.[27] Hence, the above B3LYP/BS1 obtained structures were reoptimized at the M06/BS1 level of theory. However, this caused rearrangements of the alcohol radical intermediate complex such that it no longer was able to lead to formation of the allene oxide product. In addition, relative energies were calculated at the IEFPCM-M06/6-311+G(2df,p)//B3LYP/BS1 + ΔG_{Cor} level of theory (Figure S1). Unfortunately, the resulting relative energies were found to be enzymatically unrealistic and thus are not discussed herein.

Chemical Model. The final MM minimized top scoring complex obtained above was used to generate the active site bound-substrate chemical model shown in Figure 1. In particular, it included the substrate 8(*R*)-HPETE modeled as (2E,4Z)-1-hydroperoxy-2,4-hexadiene, and the side chains of R354, T66, H67, and Y358. These were included as the side chain of R354 directly interacts with the proximal Y358 and helps stabilize the negatively charged tyrosinate. Moreover, it has been suggested that they are important for the Catalase's catalytic function.[4b,28] H67 and T66 were retained as they hydrogen bond with the substrate. Furthermore, mutation of T66 by valine causes a reduction in the catalytic activity of AOS,[4c] while H67 has been proposed to accept a proton during the mechanism (see Scheme 1). The heme's porphyrin ring was modeled by a porphine ring.

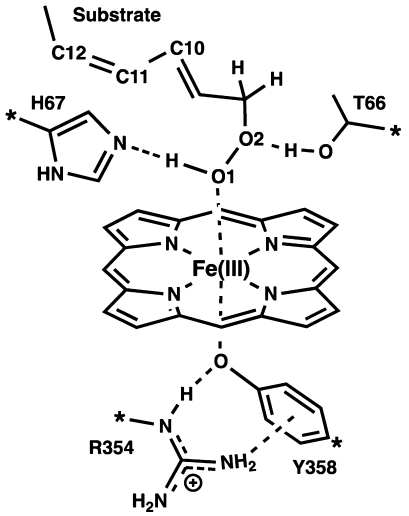

Figure 1. The active site bound-substrate model used in the investigation of AOS. Carbon atoms labeled with an asterisk were fixed to their final MM minimized position.

RESULTS AND DISCUSSION

The free energy surfaces for the overall reaction of cAOS in the *overall* doublet ($S = {}^1/_2$), quartet ($S = {}^3/_2$), and sextet ($S = {}^5/_2$) states, obtained at the IEF-PCM-B3LYP*/6-311G(2df,p)//B3LYP/BS1 + ΔG_{Cor} level of theory, are shown in Figure 2. All energies are given relative to that of the quartet reactant complex (^{4}**RC**) unless otherwise noted. The surface for the sextet state consistently lies higher in energy than those obtained for the doublet and quartet states. Hence, it is unlikely to contribute to the catalytic mechanism of cAOS. It is noted that this is in contrast to that obtained by Cho et al.[5] in which their initial complex of enzyme with an unbound peroxide substrate (see Introduction) was found to prefer the sextet state. Thus, structures and energies corresponding to this state are not discussed hereafter.

The Catalytic Mechanism of cAOS, without Dispersion Corrections. For the initial reactant complex (**RC**) the quartet state (^{4}**RC**) is preferred over ^{2}**RC** with the latter lying 11.2 kJ mol^{-1} higher in energy (Figure 2). The calculated spin densities (SD) for ^{2}**RC** and ^{4}**RC** are 0.98 and 2.95, respectively (Table 1). These values indicate that in both complexes the unpaired electrons are effectively centered on the Fe. Structurally, in ^{2}**RC** and ^{4}**RC** the *r*(Fe···O1O2) distances are 1.88 and 2.85 Å, respectively (Figure 3). That is, in the doublet state the Fe···O1 interaction is quite strong while in the quartet state it is significantly reduced. In contrast, in a previous study on pAOS no stable initial active site-bound substrate could be found.[5] This may be due to the fact that in their investigation the basis set used (i.e. LACVP) included no polarization functions.

In ^{2}**RC**, due to the strong Fe···O1 interaction, the proton on the substrate's peroxide moiety has transferred onto the imidazole of H67 (Figure 3). In contrast, in ^{4}**RC** the peroxide moiety remains protonated. In either case, however, there exists a strong hydrogen bond between the peroxy moiety and H67; in ^{2}**RC** *r*(H67−$N_\varepsilon H^+$···O1) = 1.57 Å while in ^{4}**RC** *r*(H67−N_ε···H−O1) = 1.61 Å. Notably, despite the differences in the strength of the Fe···O1 interaction the O1−O2 and C8−O2 bond lengths in ^{2}**RC** and ^{4}**RC** are not significantly different (see Figure 3). Furthermore, to help position the substrate, in both reactant complexes T66 forms a hydrogen bond to the

dx.doi.org/10.1021/jp403405b | J. Phys. Chem. B XXXX, XXX, XXX−XXX

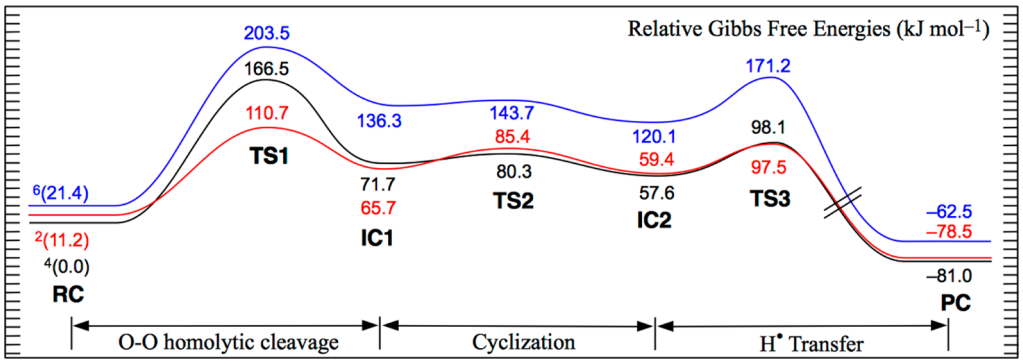

Figure 2. Free energy surfaces for the overall catalytic mechanism of cAOS obtained at the IEF-PCM-B3LYP*/6-311+G(2df,p)//B3LYP/BS1 + ΔG_{Cor} level of theory. Surface color code: red (doublet); black (quartet); and blue (sextet).

Table 1. Spin Densities on Select Atoms Obtained at the B3LYP*/6-311+G(2df,p) Level of Theory

complex	Fe	Por	O1[a]	O2[a]	C10[a]	C11[a]	C12[a]
^{2}**RC**	0.98	−0.05	0.07	0.00	0.00	0.00	0.00
^{4}**RC**	2.95	−0.10	0.00	0.00	0.00	0.00	0.00
^{2}**IC1**	1.47	−0.11	0.52	−0.66	−0.06	0.02	−0.06
^{4}**IC1**	1.48	−0.10	0.60	0.74	0.05	−0.02	0.05
^{2}**IC2**	1.43	−0.10	0.64	−0.07	−0.63	0.27	−0.65
^{4}**IC2**	1.43	−0.10	0.64	0.07	0.63	−0.27	0.65
^{2}**PC**	1.00	−0.06	0.01	0.00	0.00	0.00	0.00
^{4}**PC**	2.83	−0.05	0.04	0.00	0.00	0.00	0.00

[a]Atom labels are defined in Figure 1.

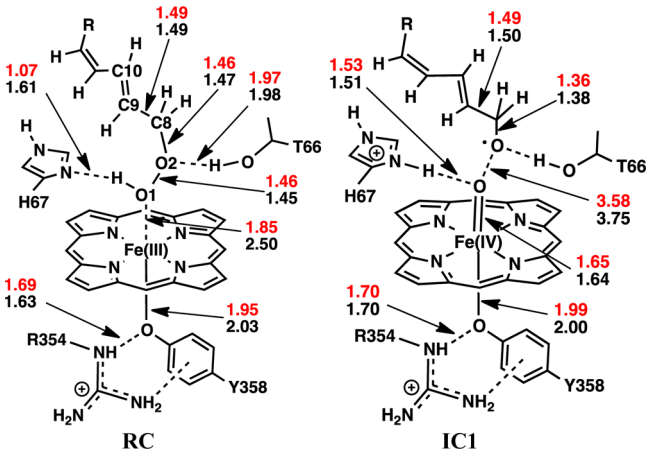

Figure 3. The optimized structures, with selected bond lengths in angstroms (Å), of **RC** and **IC1** for the $S = {}^1/_2$ (doublet: red values) and ${}^3/_2$ (quartet: black values) states.

peroxide moiety with r(T66−OH···O2) distances of 1.97 (^{2}**RC**) and 1.98 Å (^{4}**RC**).

The proximal tyrosyl ligand forms a reasonably strong interaction via its negatively charged phenolic oxygen with the Fe center in both reactant complexes with r(Y358−O···Fe) = 1.95 and 2.03 Å for the doublet and quartet states, respectively. Simultaneously, it also forms a strong hydrogen bond with the side-chain guanidinium of the arginyl residue R354 with r(R354−N$_\varepsilon$H$^+$···O−Y358) = 1.69 and 1.63 Å in ^{2}**RC** and ^{4}**RC**, respectively. It has been suggested[4b,28] that R534 is important in the mechanism of cAOS due its involvement in the Catalase mechanism function. Indeed, removal of the presence of R354 from the QM model significantly perturbed the Y358−O···Fe interaction. For example, in ^{2}**RC** it led to significant lengthening in r(Y358−O···Fe) of 0.55 Å.

The first step along the overall mechanism is cleavage of the peroxy bond. This occurs via ^{2}**TS1** and ^{4}**TS1** with free energy barriers of 110.7 and 166.5 kJ mol^{-1}, respectively (Figure 2). Both of these barriers are considerably higher than that previously obtained for pAOS in the doublet state of 75.7 kJ mol^{-1}.[5] If only the doublet surface is considered for cAOS then the currently calculated barrier for cleavage is only 99.5 kJ mol^{-1}. Importantly, however, in cAOS ^{4}**RC** is the lowest free energy reactant complex. Hence, it appears that cleavage of the peroxy bond preferably occurs with spin inversion (SI) from the quartet to doublet surface. Notably, the occurrence of SI has been suggested to be common in transition metal chemistry.[7]

In ^{2}**TS1** and ^{4}**TS1** the O1···O2 peroxy bond has lengthened considerably by at least 0.24 Å to 1.87 and 1.71 Å, respectively (Figure S3). In the latter case (^{4}**TS1**) the substrate's peroxide proton transfers to His67 concomitant with peroxide bond cleavage. That is, in both the doublet (in ^{2}**RC**) and quartet (in ^{4}**TS1**) state the substrate's hydroperoxy proton is transferred to the imidazole of His67 early in the overall mechanism to give a protonated His67 (His67−H$^+$). This suggests that the experimentally proposed[4a] role of His67 as the base that abstracts a proton during the later reduction of the Cpd II intermediate is unlikely (Scheme 1). Notably, the transition structures have markedly different electronic configurations on their Fe centers compared to the corresponding reactive complexes. Consequently, the Fe−O1−O2 angles in ^{2}**TS1** and ^{4}**TS1** of 122.5° and 168.7°, respectively, vary significantly by 6.2° and 54.9°, respectively, relative to their corresponding reactive complexes (Table S1).

For both the doublet and quartet states the resulting intermediate formed (**IC1**) is an oxo-ferryl Cpd II type intermediate (i.e. Pro(Fe(IV)═O) with ^{2}**IC1** lying 6.0 kJ mol^{-1} lower in energy than ^{4}**IC1**. For both states, however, formation of Cpd II is endergonic with ^{2}**IC1** and ^{4}**IC1** lying 65.7 and 71.7 kJ mol^{-1} higher in energy than ^{4}**RC**, respectively (Figure 2). The optimized Fe(IV)═O bond lengths in ^{2}**IC1** and ^{4}**IC1** are quite short at 1.65 and 1.64 Å, respectively, indicating that they have considerable double bond character (Figure 3). Conversely, the now cleaved O1···O2 distance has lengthened considerably to 3.58 (^{2}**IC1**) and 3.75 (^{4}**IC1**) Å, respectively. Only quite minor changes in the Y358−O···Fe interaction length are observed upon forming Cpd II. As can be seen in Table 1, there is very little or no spin density (SD) observed on either the tyrosyl or porphyrin ring. In contrast,

dx.doi.org/10.1021/jp403405b | J. Phys. Chem. B XXXX, XXX, XXX−XXX

the SDs on the Fe center of 1.47 (^{2}**IC1**) and 1.48 (^{4}**IC1**) suggest that the oxo-ferryl center likely has a pair of unpaired electrons (i.e. triplet) with parallel spin in both complexes. Furthermore, the Fe-bound oxygen has SDs of 0.52 and 0.60, respectively. For the alkoxy intermediate its total SDs are calculated to be −0.93 (^{2}**IC1**) and 0.99 (^{4}**IC1**) with the spin density predominantly localized on the oxygen radical itself, which has SDs of −0.66 and 0.74, respectively. However, despite a shortening and strengthening of the T66−OH···O2 interaction and hence stabilization of the intermediates oxygen radical center (O2), spin delocalization is observed. Notably, the hydrogens geminal to O2 are calculated to now have a marked increase in SDs. This delocalization is also evidenced by the fact that its r(C8−O2$^\bullet$) bond has shortened considerably by ∼0.1 Å in both states.

The above Cpd II intermediate differs from that calculated for pAOS which, due in part to the lack of an active site histidyl, was protonated and consequently exhibits a considerably longer Fe−O bond length of 1.87 Å.[5] Furthermore, it was a biradical with essentially no spin density on the Fe−O oxygen but significant SD on the proximal Fe-ligating sulfhydryl (−0.24) and porphyrin ring (−0.88).[5]

The next step is cyclization of the alkoxy radical to form an epoxide. This occurs via ^{2}**TS2** and ^{4}**TS2** (Figure S3) with a Gibbs barrier of 19.7 and 8.6 kJ mol^{-1} relative to ^{2}**IC1** and ^{4}**IC1**, respectively. The resulting epoxide-containing Cpd II intermediates (**IC2**) are just 59.4 and 57.6 kJ mol^{-1} higher than ^{4}**RC** on the doublet and quartet surfaces, respectively (Figure 2). That is, epoxide formation is an exergonic process as they lie lower in free energy than their corresponding **IC1** complex by −6.3 and −14.1 kJ mol^{-1} for the doublet and quartet states, respectively. Cyclization causes both the C8−O2 and C10−C9 bonds to lengthen considerably with the latter having lost its double bond character (Figure 4). Furthermore, the unpaired

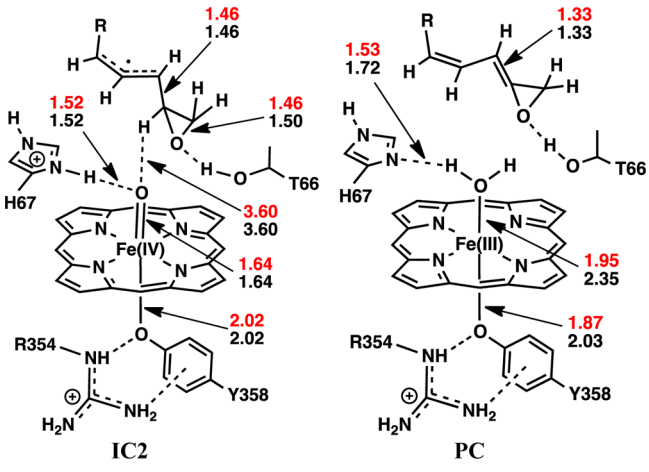

Figure 4. The optimized structures, with selected bond lengths in angstroms (Å), of **IC2** and **PC** for the $S = {}^1/_2$ (doublet: red values) and ${}^3/_2$ (quartet: black values) states.

electron of the former alkoxy radical now exists as an allylic radical delocalized on carbons C10, C11, and C12 as indicated by the SDs given in Table 1. In the case of the Cpd II moiety itself, epoxide has an insignificant effect on its geometry.

The final step is the generation of the allene oxide via the removal of a H$^\bullet$ from the epoxides C9−H group. However, the Fe═O···H—C9 distance in **IC2** is approximately 3.60 Å for both the doublet and quartet states (Figure 4). Thus, in the transition structure for this process (**TS3**) the epoxide allylic radical has shifted markedly closer to the Fe(IV)═O moiety. However, it was found that the His67−H$^+$ proton, which is hydrogen bonded to the Fe-bound oxygen in **IC2** (Figure 4), has now essentially transferred to the oxo-ferryl moiety as indicated by the relatively short r(Fe−O···H$^+$) distances of 1.00 and 1.01 Å in ^{2}**TS3** and ^{4}**TS3**, respectively (Figure S3). Thus, in either **TS3** the iron−oxygen moiety is perhaps better describe as an Fe(IV)−OH that is now involved in H$^\bullet$ abstraction from the epoxide radical. In ^{2}**TS3** the FeO1···H$^\bullet$ distance has shortened to 1.56 Å while the H$^\bullet$···C9 bond has elongated to 1.17 Å. On the quartet free energy surface, ^{4}**TS3** appears to occur notably later along the reaction coordinate as suggested by its markedly shorter FeO1···H$^\bullet$ distance of 1.38 Å and concomitantly significantly more elongated H$^\bullet$···C9 distance of 1.24 Å. Despite such structural changes the free energies for ^{2}**TS3** and ^{4}**TS3** are only 38.1 and 40.5 kJ mol^{-1} relative to their corresponding **IC2** complexes (Figure 2).

Complete transfer of the hydrogen atom, i.e. formation of the product complex (**PC**), results in the C10−C9 bond shortening considerably due to restoration of its double bond character. Concomitantly, the C10−C9−C8−O2 torsional angle has increased to 176.9° and 178.0° in ^{2}**PC** and ^{4}**PC**, respectively, indicating near planarity of the allene oxide functional group. Importantly, with the H$^\bullet$ fully transferred onto the Fe-bound $^-$OH group an Fe-bound water has been formed (Figure 4). As a result, the Fe···O1H$_2$ distance has increased to 1.95 and 2.35 Å in ^{2}**PC** and ^{4}**PC**, respectively. It is noted that, similar to that observed for the reactant complexes ^{2}**RC** and ^{4}**RC**, the calculated spin densities (SD) of ^{2}**PC** and ^{4}**PC** indicate that the unpaired electrons are essentially centered on the Fe(III) metal ion (Table 1). In particular, for ^{2}**PC** and ^{4}**PC** the calculated SDs on the Fe are 1.00 and 2.83, respectively. The relative free energies of ^{2}**PC** and ^{4}**PC** are markedly lower than that of ^{4}**RC** by 78.5 and 81.0 kJ mol^{-1}, respectively (Figure 2). That is, the overall formation of allene oxide via a PCET mechanism as catalyzed by cAOS is exergonic.

The above free energy surfaces suggest that the mechanism of cAOS may involve multistate reactivity (MSR).[18b] More specifically, the reaction begins in the quartet state with ^{4}**RC**. Then, a spin inversion occurs allowing for a more facile O−O cleavage on the doublet surface via ^{2}**TS1**. More specifically, the barrier for this process on the doublet surface is 55.8 kJ mol^{-1} *lower* in free energy than would otherwise be required on the quartet surface (Figure 2)! It should be noted that given that ^{4}**PC** lies lower in free energy than ^{2}**PC** a second SI likely occurs later in the mechanism and prior to final product formation. Thus, the use of a common "noncorrected" computational approach to investigating enzymatic processes suggests that the reaction of cAOS requires the use of MSR.[18b] It is noted that regardless of the possible SI processes, the overall mechanism of cAOS is calculated to occur with considerably higher Gibbs free energies than that obtained previously[5] for the analogous pathway in pAOS. In particular, the free energies for the entire process (Figure 2) are on average 30.2 kJ mol^{-1} higher than those for pAOS,[5] the most significant difference occurring for the H$^\bullet$ abstraction process (i.e. **TS3**). Potentially this difference may be due to the presence of a ligating tyrosyl residue in cAOS rather than the cysteinyl in pAOS resulting in a more reactive Cpd II intermediate. It is noted that these energetic differences may also partly be due to the differences in the computational models used (i.e., B3LYP*-based QM-cluster versus use of B3LYP within a QM/MM framework[5]). However,

dx.doi.org/10.1021/jp403405b | J. Phys. Chem. B XXXX, XXX, XXX−XXX

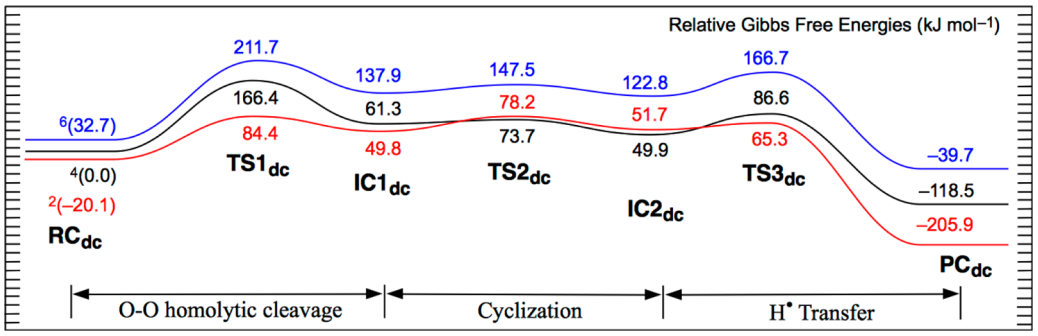

Figure 5. Schematic illustration of the dispersion-corrected free energy surfaces obtained at the IEF-PCM-B3LYP*/6-311+G(2df,p) + ΔG_{Cor} + $\Delta Disp_{Cor}$ level of theory for the overall catalytic mechanism of cAOS. Surface color code: red (doublet); black (quartet); and blue (sextet).

as noted above the Cpd II intermediate of cAOS differs from that calculated for pAOS, which was found to be biradical with essentially no spin density on the Fe−O oxygen but significant SD on the proximal Fe-ligating sulfhydryl (−0.24) and porphyrin ring (−0.88).[5]

As noted in the Introduction, however, noncovalent interactions often dominate in the interactions between ligands and proteins.[8] Furthermore, previous investigations of P450-enzymes have suggested that the barriers for the reactions were considerably affected by the inclusion of corrections for dispersion interactions.[11]

The Effects of Including Dispersion Corrections. The effect of dispersion interactions was modeled by, as described in the Computational Methods, inclusion of a dispersion correction ($\Delta Disp_{Cor}$) to the above free energy surfaces. The resulting corrected free energy surfaces for the doublet, quartet, and sextet states are presented in Figure 5. Again, the sextet surface is calculated to lie significantly higher in energy for all complexes and transition structures along the enzymes mechanistic pathway. In fact, inclusion of $\Delta Disp_{Cor}$ has effectively raised the relative energies of all but one of the sextet species by 1.6 (**IC1**) to 22.8 (**PC**) kJ mol^{-1} with respect to ^{4}**RC**$_{dc}$ (cf. Figure 2). The only exception is **TS3**, which decreases by 4.5 kJ mol^{-1}. This simply reflects that all sextet species except **TS3** are stabilized to a lesser extent by dispersion interactions than ^{4}**RC**$_{dc}$ (see below). Hence, unless otherwise noted discussion is herein limited to the doublet and quartet surfaces.

Upon correcting for dispersion interactions ^{2}**RC** is stabilized by 31.3 kJ mol^{-1} relative to ^{4}**RC**. In fact, in contrast to that seen for the uncorrected free energies (cf. Figure 2) ^{2}**RC**$_{dc}$ now lies *lower* in energy than ^{4}**RC**$_{dc}$ by 20.1 kJ mol^{-1} (Figure 5)! This preferential stabilization of ^{2}**RC**$_{dc}$ relative to ^{4}**RC**$_{dc}$ is likely due to the fact that in the former the hydroperoxy substrate is significantly more tightly ligated to the heme Fe center (Figure 3). If we consider the distance between centers of mass for the hydroperoxy substrate and porphine ring (Figure S2) we find a difference of 0.362 Å. As a consequence, the dispersion interactions between the substrate's carbon chain and the heme are greater. This enhanced stabilization is also observed, though to a lesser extent, in the transition structure for homolytic O−O bond cleavage of **TS1**$_{dc}$ (Figure 2). Specifically, the free energy barrier for this step is now lowered by 6.2 kJ mol^{-1} relative to ^{2}**RC**$_{dc}$ (a stabilization of 26.3 kJ mol^{-1} relative to ^{2}**RC**$_{dc}$). Regardless of this stabilization, O−O homolytic cleavage remains the rate-limiting step in the overall mechanism on both the doublet and quartet surfaces. Importantly, this reordering of states suggests that spin inversion (SI) is not necessary for O−O cleavage given this occurs lowest on the doublet surface with a Gibbs barrier of 104.5 kJ mol^{-1} (Figure 5). For the resulting Cpd II intermediate **IC1**, opposite effects appear to be seen for the doublet and quartet states. More specifically, ^{2}**IC1**$_{dc}$ appears to be destabilized by 15.4 kJ mol^{-1} relative to ^{2}**RC**$_{dc}$ while ^{4}**IC1**$_{dc}$ appears to be stabilized by 10.4 kJ mol^{-1} relative to the initial reactant complex ^{4}**RC**$_{dc}$. However, this is due to the fact than ^{2}**RC**$_{dc}$ is significantly stabilized by dispersion interactions due to tighter binding of the substrate to the heme. But, upon O−O bond cleavage the alkoxy radical formed is shifted away from the heme and hence ^{2}**IC1**$_{dc}$ and later stationary points along the mechanism pathway are *less* stabilized by dispersion interactions (Figure 3). However, we do see slightly greater stabilization of ^{2}**IC1** with respect to ^{4}**IC1** when dispersion effects are included (i.e. ^{2}**IC1**$_{dc}$ lies 11.5 kJ mol^{-1} lower in energy than ^{4}**IC1**$_{dc}$ as opposed to only 6.0 kJ mol^{-1} seen in Figure 2). This can be better understood if we again consider the distance between centers of mass for the alkoxy radical and porphine ring. In particular, like the reactive complexes we find the intermediate is slightly closer to the porphine ring for the doublet system than the quartet system where a difference of 0.211 Å was found (Figure S2).

The barriers for conversion of **IC1**$_{dc}$ into the alternate Cpd II species **IC2**$_{dc}$ via **TS2**$_{dc}$ are 28.4 and 12.4 kJ mol^{-1} for the doublet and quartet surfaces, respectively (Figure 5). Notably, ^{4}**TS2**$_{dc}$ lies 3.5 kJ mol^{-1} lower in energy than ^{2}**TS2**$_{dc}$. Furthermore, unlike that observed for the order of the states for **IC1**$_{dc}$, ^{4}**IC2**$_{dc}$ lies lower in energy than ^{2}**IC2**$_{dc}$ by 1.8 kJ mol^{-1}. Notably, as seen in Figure 2, ^{4}**IC2** also lies 1.8 kJ mol^{-1} lower in energy than ^{2}**IC2**. If we again consider the distance between centers of mass for the allylic epoxide radical intermediate and porphine ring we find an insignificant difference of 0.001 Å (Figure S2). Thus, as seen in Figure 2, multistate reactivity could potentially play a role in interconversion of the two mechanistic Cpd II species with the quartet surface providing a slightly lower energy pathway (Figure 5).

As observed for the nondispersion corrected surfaces (Figure 2), the dispersion corrected barriers for the final step are again lower on the doublet surface than on the quartet surface. However, now the difference is much greater with ^{2}**TS3**$_{dc}$ lying lower in energy than ^{4}**TS3**$_{dc}$ by 21.3 kJ mol^{-1}. That is, the final reaction step once again preferentially proceeds via a possible spin inversion from the quartet to doublet surface. Notably, in contrast to that observed for the uncorrected free energy surfaces (cf. Figure 2), the inclusion of dispersion effects leads to the suggestion that the overall mechanism of cAOS could

dx.doi.org/10.1021/jp403405b | J. Phys. Chem. B XXXX, XXX, XXX−XXX

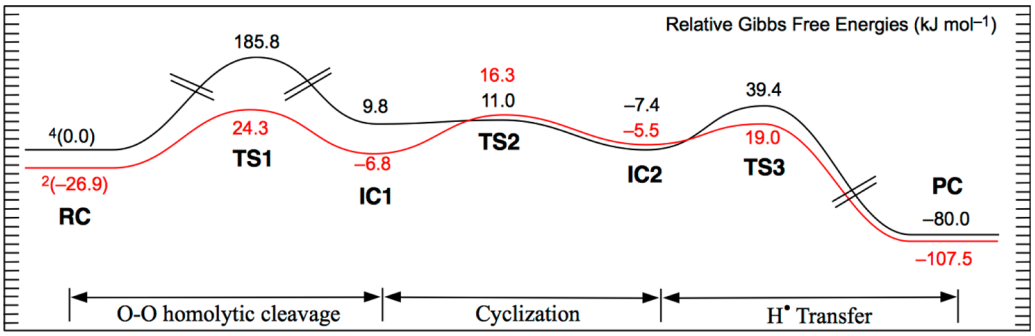

Figure 6. Free energy surfaces for the catalytic mechanism of cAOS obtained at the IEF-PCM-BP86/6-311G(2df,p)//B3LYP*/BS1 + ΔG_{cor} level of theory. Surface color code: red (doublet; $S = {}^1/_2$) and black (quartet; $S = {}^3/_2$).

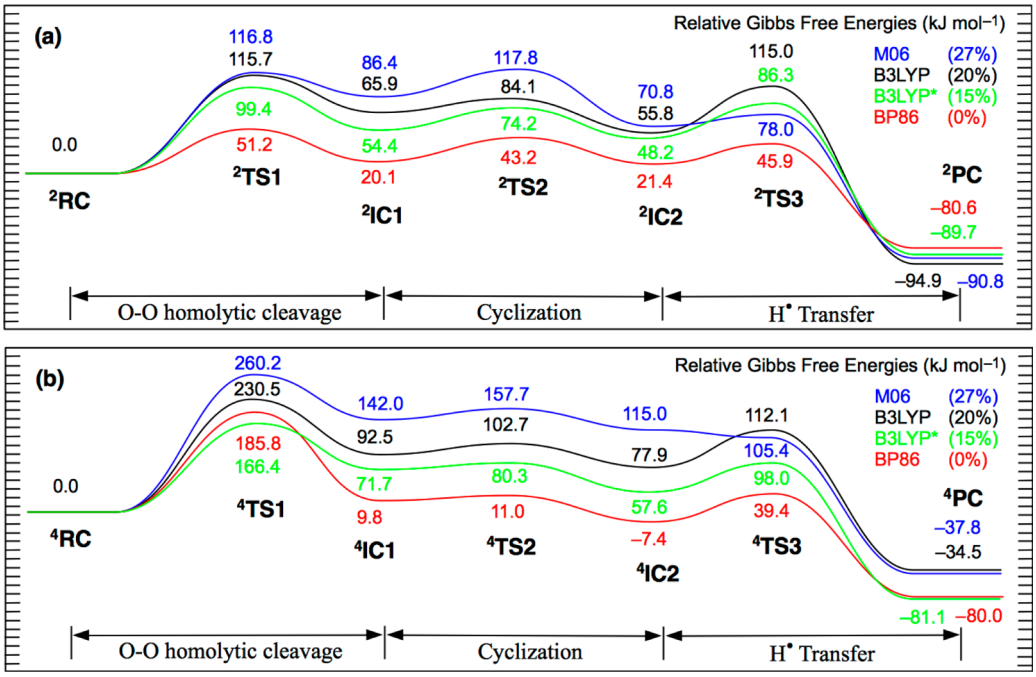

Figure 7. Free energy surfaces for the catalytic mechanism of cAOS obtained at the IEF-PCM-DFT$_i$/6-311G(2df,p)//B3LYP*/BS1 + ΔG_{cor} level of theory (DFT$_i$ = M06, B3LYP, B3LYP*, and BP86): (a) doublet ($S = {}^1/_2$) state and (b) quartet ($S = {}^3/_2$) state. The values given in parentheses indicate the %HF contribution in the functional.

occur *without* the necessity of a spin inversion from the doublet to quartet surfaces. For the product complexes, and in contrast without correcting for dispersion interactions (Figure 2), $^2\mathbf{PC}_{dc}$ now lies lower in energy than $^4\mathbf{PC}_{dc}$ by 87.4 kJ mol^{-1}! That is, similar to the reactive complexes, accounting for dispersion interactions results in a reordering of the states for the product complex. If we consider the distance between centers of mass for the allene oxide product and porphine ring (Figure S2) we find a difference of 0.713 Å! Hence, $^2\mathbf{PC}_{dc}$ is strongly stabilized by such effects due to the allene oxide itself being considerably closer to the heme ring in $^2\mathbf{PC}_{dc}$ compared to $^4\mathbf{PC}_{dc}$. Like the previous situation the overall mechanism of cAOS with dispersion corrections (with the exception of $^2\mathbf{PC}$) is calculated to occur with higher Gibbs free energies than that obtained previously[5] for the analogous pathway in pAOS. In particular, the free energies for the entire process (excluding $^2\mathbf{PC}$) are on average 37.3 kJ mol^{-1} higher than those for pAOS.[5]

The Effects of Choice of DFT Functional. As recently discussed by Ye and Neese[29] the ordering of spin states can be sensitive to the functional chosen. More specifically, they investigated several inorganic complexes that have been shown to be problem cases for DFT methods.[29] They concluded that in general the B2PLYP functional in conjunction with large and flexible basis sets gave the best qualitative agreement with experiment.[29] However, for complexes containing strong-field ligands all DFT methods employed predicted the correct ground-state multiplicity.[29] Reiher et al.[25] have shown that the relative ordering of states is sensitive to the amount of the HF contribution. In particular, they concluded that the most reliable description of transition-metal complexes with sulfur-rich first coordination spheres was obtained when the HF contribution in B3LYP was reduced to 15%.[25] Notably, in heme systems the ligands that bind the Fe center are typically characterized as strong field ligands.[30]

Thus, we also investigated the mechanism of cAOS using the GGA functional (i.e., 0% HF contribution), BP86. It is noted that DCPs were not developed for use with BP86 hence the relative free energies were obtained at the IEF-PCM-BP86/6-311G(2df,p)//B3LYP*/BS1 + ΔG_{cor} level of theory and are given in Figure 6. However, the corresponding free energy surface in which $\Delta Disp_{Cor}$ has been included is provided in Figure S2.

dx.doi.org/10.1021/jp403405b | J. Phys. Chem. B XXXX, XXX, XXX−XXX

As can be seen in Figure 6, the use of the BP86 functional results in ^{4}**RC** no longer being the most favored state. Instead, it now lies 26.9 kJ mol^{-1} higher in energy than ^{2}**RC**. Furthermore, the relative free energy of **PC** is also now lowest for the doublet state. Interestingly, however, while the relative ordering of the states of **RC** and **PC** is reversed compared to that obtained by using B3LYP* (Figure 2), those of the remaining stationary points along the pathway are not. For example, in the case of **TS2** and **IC2** the quartet state is still lower in energy compared to the doublet state. Importantly, with use of the BP86 functional the barrier for O−O homolytic cleavage in the $S = {}^1/_2$ state is significantly lower at only 51.2 kJ mol^{-1}. In contrast, by using the B3LYP* functional this same reaction has a calculated barrier of 110.7 kJ mol^{-1} (Figure 2). Furthermore, the use of the BP86 functional suggests that in order to be enzymatically feasible the mechanism of cAOS does not appear to require the involvement of MSR.

To better compare the effect of changing functional on each of the free energy surfaces for both the doublet and quartet states, the overall mechanisms obtained at the IEF-PCM-DFT$_i$/6-311G(2df,p)//B3LYP*/BS1 + ΔG_{cor} level of theory (DFT$_i$ = M06, B3LYP, B3LYP*, and BP86) for each state are shown in Figure 7. As can be seen, the results suggest that for both states there is a correlation between the amount of %HF contribution in the functional and the reduction in the relative energies of the stationary points along the pathway. For both states when we change the functional from M06 to B3LYP we see an average reduction in relative free energies of 6.2 and 26.9 kJ mol^{-1} for the doublet ($S = {}^1/_2$) and quartet ($S = {}^3/_2$) states, respectively. Reducing the %HF contribution in B3LYP from 20% to 15% (i.e., on changing from B3LYP to B3LYP*) further average reductions are observed of 12.0 (doublet) and 31.4 (quartet) kJ mol^{-1}. Lastly, on changing the functional from B3LYP* to BP86 further average reductions in the relative energies are observed of 28.1 and 39.1 kJ mol^{-1} for the doublet ($S = {}^1/_2$) and quartet ($S = {}^3/_2$) states, respectively. That is, for both states as the %HF contribution is reduced, so are in general the relative free energies of the various stationary points along the surface (relative to **RC**). In fact, overall, the average reduction in relative energies obtained upon going from the M06 to BP86 functional are 46.3 and 97.3 kJ mol^{-1} for the doublet and quartet states, respectively. The largest change on both surfaces occurs for **TS2**, which sees a lowering in its relative energy of 74.6 (^{2}**TS2**) and 146.7 (^{4}**TS2**) kJ mol^{-1}! Thus, comparison of the results obtained by using the B3LYP* (Figure 2), BP86 (Figure 6), and M06 (Figure S1) functionals suggests that the mechanism of cAOS is also sensitive to the choice of functional, with the quartet state being most affected.

Interestingly, from Figure 7 it can be seen that the M06 functional predicts a higher barrier for O−O cleavage (i.e. **TS1**) in comparison to the other three functionals. However, for the same functional the relative energy of **TS3** with respect to **IC2** is considerably less than that obtained with the other functionals. In particular, ^{4}**TS3** actually lies lower in energy than ^{4}**IC2**. This indicates that using the M06 functional, and in contrast to that obtained by using any of the other functionals, the final step of the mechanism is predicted to occur essentially without a barrier at 298 K on the quartet surface. That is, after cyclization of the alkoxy radical, H$^\bullet$ abstraction from the epoxide intermediate by Cpd II is predicted to readily occur. On the doublet surface (Figure 7a) ^{2}**TS3** lies slightly higher in energy than ^{2}**IC2** by only 7.2 kJ mol^{-1}. Thus, for either state use of the M06 functional leads to the prediction of a low barrier for H$^\bullet$ abstraction by Cpd II. Overall, however, the most thermodynamically and kinetically favorable free energy surfaces, but still qualitatively correct, are obtained by using the BP86 functional (i.e., IEF-PCM-BP86/6-311G(2df,p)//B3LYP*/BS1 + ΔG_{cor} level of theory). That is, the functional with the lowest %HF contribution (0%) in general gives the lowest relative energies (with respect to **RC**) of the intermediates and transition structures. In contrast, M06 has the highest %HF contribution (27%) of the four functionals considered herein and in general gives the highest relative free energies of the intermediates and transition structures with respect to **RC**.

CONCLUSIONS

In this present work the mechanism by which coral allene oxide synthase (cAOS) catalyzes the formation of allene oxide from its hydroperoxy substrate has been computationally investigated by using a DFT-chemical cluster approach. Specifically, we have examined the effect of dispersion interactions and multistate reactivity along the mechanism, and the effect of the tyrosyl proximal ligand of cAOS compared to the cysteinyl found in pAOS.

In the reactant complex (**RC**) the hydroperoxy substrate forms a strong Fe−O−O−C cross-link in the overall $S = {}^1/_2$ (doublet) state with r(Fe−O) = 1.85 Å. In contrast, in the overall $S = {}^3/_2$ (quartet) state this link is much weaker with r(Fe−O) = 2.50 Å. Regardless, the overall mechanism begins with cleavage of the peroxy O−O bond to give a Cpd II-type intermediate with concomitant formation of an alkoxy radical. Subsequently, the latter species undergoes a rearrangement to give an epoxide with a delocalized allylic radical. The final step is hydrogen abstraction from the epoxide to give an Fe-bound H_2O and an epoxide. Thus, cAOS utilizes a mechanism that is similar to that for pAOS.

The mechanism of cAOS, however, appears to differ from that of pAOS in several key features. In particular, the initial Cpd II intermediate formed has a markedly different overall electronic configuration to that calculated for pAOS. This is likely due to both the presence of a histidyl active site residue in cAOS, which is lacking in pAOS, and a ligating tyrosyl residue. Furthermore, the mechanism occurs with considerably higher Gibbs free energies of reaction than that for the analogous pathway in pAOS. However, it is noted that these energetic differences may be partly due to differences in the computational models used to previously[5] study pAOS versus that used herein.

From the results obtained at the IEF-PCM-B3LYP*/6-311+G(2df,p)//B3LYP/BS1 + ΔG_{Cor} level of theory the inclusion of dispersion effects results in considerable changes to the free energy surface for the mechanism. For instance, without dispersion effects the homolytic O−O bond cleavage likely occurs with SI from the quartet to doublet surface. However, with dispersion corrections the energy ordering of the various states of RC is altered such that SI is not needed for the initial step as the overall $S = {}^1/_2$ (doublet-state) reactive complex (i.e. ^{2}**RC**$_{dc}$) is now most favored. Similarly, the occurrence of SI in product formation is also now unlikely to occur when dispersion effects are included due in part to reordering of the relative free energies of the product complexes; ^{2}**RC**$_{dc}$ is now significantly more favored. The contribution of dispersion effects directly correlates with the changes observed along the mechanisms pathway with regards

dx.doi.org/10.1021/jp403405b | J. Phys. Chem. B XXXX, XXX, XXX−XXX

to the distance between the center of mass of the substrate and heme.

Thus, in contrast to that observed for the uncorrected free energy surfaces (i.e., at the IEF-PCM-B3LYP*/6-311+G(2df,p)//B3LYP/BS1 + ΔG_{Cor} level of theory) the inclusion of dispersion effects leads to the suggestion that the overall mechanism of cAOS could occur *without* the need for spin inversion. Importantly, the present investigation infers that while energetic differences may exist due to the various electronic configurations of the Fe center subtle effects such as the vdW distances between substrate and enzyme can also significantly affect the energetics. Importantly, such effects may result in very different qualitative and quantitative results as shown here.

In addition we investigated the effect of changing functional (i.e., at the IEF-PCM-DFT$_i$/6-311+G(2df,p)//B3LYP/BS1 + ΔG_{Cor} level of theory; DFT$_i$ = M06, B3LYP, B3LYP*, BP86) on the free energy surfaces for both the doublet and quartet states. For both states there is in general a correlation between the amount of %HF contribution in the functional and the reduction in the relative energies of the stationary points along the pathway. That is, the functional with the lowest %HF contribution (0%) in general gives the lowest relative free energies (with respect to **RC**) of the intermediates and transition structures. In contrast, M06, which has the highest % HF contribution (27%) of the four functionals considered herein, in general gives the highest relative free energies of the intermediates and transition structures with respect to **RC**. In fact, the average reduction in relative free energies obtained upon going from the M06 to BP86 functional is 46.3 and 97.3 kJ mol^{-1} for the doublet and quartet states, respectively.

■ ASSOCIATED CONTENT

Ⓢ Supporting Information

The free energy surfaces for the calculations performed at IEF-PCM-M06/6-311+G(2df,p)//B3LYP/BS1 + ΔG_{Cor} level of theory, schematic illustration of the distances between centers of mass of the substrate and porphine ring, the optimized structures, with selected bond lengths in angstroms, of **TS1**, **TS2**, and **TS3**, and XYZ's for the optimized structures on the doublet, quartet, and sextet states. This material is available free of charge via the Internet at http://pubs.acs.org.

■ AUTHOR INFORMATION

Corresponding Author

*E-mail: gauld@uwindsor.ca.

Notes

The authors declare no competing financial interest.

■ ACKNOWLEDGMENTS

We thank the Natural Sciences and Engineering Research Council of Canada (NSERC), SHARCNET, and Compute Calcul Canada for additional computational resources and graduate scholarships (E.A.C.B.). E.A.C.B. also thanks NSERC for a PGS-D Scholarship.

■ REFERENCES

(1) (a) Caldwell, G. S. The Influence of Bioactive Oxylipins from Marine Diatoms on Invertebrate Reproduction and Development. *Mar. Drugs* **2009**, *7* (3), 367−400. (b) Sebolai, O. M.; Pohl, C. H.; Kock, L. J. F.; Chaturvedi, V.; del Poeta, M. The presence of 3-hydroxy oxylipins in pathogenic microbes. *Prostaglandins Other Lipid Mediators* **2012**, *97* (1−2), 17−21. (c) Vera, J.; Castro, J.; Gonzalez, A.; Moenne, A. Seaweed Polysaccharides and Derived Oligosaccharides Stimulate Defense Responses and Protection Against Pathogens in Plants. *Mar. Drugs* **2011**, *9* (12), 2514−2525. (d) Brodhun, F.; Feussner, I. Oxylipins in fungi. *FEBS J.* **2011**, *278* (7), 1047−1063. (e) Tsitsigiannis, D. I.; Keller, N. P. Oxylipins as Developmental and Host-Fungal Communication Signals. *Trends Microbiol.* **2007**, *15* (3), 109−118.

(2) Andreou, A.; Brodhun, F.; Feussner, I. Biosynthesis Of Oxylipins In Non-Mammals. *Prog. Lipid Res.* **2009**, *48* (3−4), 148−170.

(3) (a) Boutaud, O.; Brash, A. R. Purification And Catalytic Activities Of The Two Domains Of The Allene Oxide Synthase-Lipoxygenase Fusion Protein Of The Coral Plexaura Homomalla. *J. Biol. Chem.* **1999**, *274* (47), 33764−33770. (b) Feussner, I.; Wasternack, C. The lipoxygenase pathway. *Annu. Rev. Plant Biol.* **2002**, *53*, 275−297. (c) Grechkin, A. Recent Developments In Biochemistry Of The Plant Lipoxygenase Pathway. *Prog. Lipid Res.* **1998**, *37* (5), 317−352. (d) Gao, B.; Boeglin, W. E.; Brash, A. R. Role Of The Conserved Distal Heme Asparagine Of Coral Allene Oxide Synthase (Asn137) And Human Catalase (Asn148): Mutations Affect The Rate But Not The Essential Chemistry Of The Enzymatic Transformations. *Arch. Biochem. Biophys.* **2008**, *477* (2), 285−290.

(4) (a) Oldham, M. L.; Brash, A. R.; Newcomer, M. E. The Structure Of Coral Allene Oxide Synthase Reveals A Catalase Adapted For Metabolism Of A Fatty Acid Hydroperoxide. *Proc. Natl. Acad. Sci. U.S.A.* **2005**, *102* (2), 297−302. (b) Abraham, B. D.; Sono, M.; Boutaud, O.; Shriner, A.; Dawson, J. H.; Brash, A. R.; Gaffney, B. J. Characterization Of The Coral Allene Oxide Synthase Active Site With UV-Visible Absorption, Magnetic Circular Dichroism, And Electron Paramagnetic Resonance Spectroscopy: Evidence For Tyrosinate Ligation To The Ferric Enzyme Heme Iron. *Biochemistry* **2001**, *40* (7), 2251−2259. (c) Tosha, T.; Uchida, T.; Brash, A. R.; Kitagawa, T. On The Relationship Of Coral Allene Oxide Synthase To Catalase − A Single Active Site Mutation That Induces Catalase Activity In Coral Allene Oxide Synthase. *J. Biol. Chem.* **2006**, *281* (18), 12610−12617.

(5) Cho, K. B.; Lai, W. Z.; Hamberg, M.; Raman, C. S.; Shaik, S. The Reaction Mechanism Of Allene Oxide Synthase: Interplay Of Theoretical QM/MM Calculations And Experimental Investigations. *Arch. Biochem. Biophys.* **2011**, *507* (1), 14−25.

(6) Lee, D. S.; Nioche, P.; Hamberg, M.; Raman, C. S. Structural Insights Into The Evolutionary Paths Of Oxylipin Biosynthetic Enzymes. *Nature* **2008**, *455* (7211), 363−U27.

(7) Poli, R.; Harvey, J. N. Spin Forbidden Chemical Reactions Of Transition Metal Compounds. New Ideas And New Computational Challenges. *Chem. Soc. Rev.* **2003**, *32* (1), 1−8.

(8) Johnson, E. R.; Keinan, S.; Mori-Sanchez, P.; Contreras-Garcia, J.; Cohen, A. J.; Yang, W. T. Revealing Noncovalent Interactions. *J. Am. Chem. Soc.* **2010**, *132* (18), 6498−6506.

(9) Siegbahn, P. E. M.; Blomberg, M. R. A.; Chen, S. L. Significant van der Weals Effects in Transition Metal Complexes. *J. Chem. Theory Comput.* **2010**, *6* (7), 2040−2044.

(10) Sousa, S. F.; Fernandes, P. A.; Ramos, M. J. General Performance Of Density Functionals. *J. Phys. Chem. A* **2007**, *111* (42), 10439−10452.

(11) (a) Lai, W.; Chen, H.; Cohen, S.; Shaik, S. Will P450(cam) Hydroxylate or Desaturate Alkanes? QM and QM/MM Studies. *J. Phys. Chem. Lett.* **2011**, *2* (17), 2229−2235. (b) Lonsdale, R.; Harvey, J. N.; Mulholland, A. J. Inclusion of Dispersion Effects Significantly Improves Accuracy of Calculated Reaction Barriers for Cytochrome P450 Catalyzed Reactions. *J. Phys. Chem. Lett.* **2010**, *1* (21), 3232−3237. (c) Lonsdale, R.; Harvey, J. N.; Mulholland, A. J. Effects of Dispersion in Density Functional Based Quantum Mechanical/Molecular Mechanical Calculations on Cytochrome P450 Catalyzed Reactions. *J. Chem. Theory Comput.* **2012**, *8* (11), 4637−4645. (d) Schyman, P.; Lai, W. Z.; Chen, H.; Wang, Y.; Shaik, S. The Directive of the Protein: How Does Cytochrome P450 Select the Mechanism of Dopamine Formation? *J. Am. Chem. Soc.* **2011**, *133* (20), 7977−7984.

(12) Hirao, H. Which DFT Functional Performs Well in the Calculation of Methylcobalamin? Comparison of the B3LYP and BP86

Functionals and Evaluation of the Impact of Empirical Dispersion Correction. *J. Phys. Chem. A* **2011**, *115* (33), 9308−9313.
(13) Hung, R. R.; Grabowski, J. J. Listening To Reactive Intermediates: Application Of Photoacoustic Calorimetry To Vitamin B-12 Compounds. *J. Am. Chem. Soc.* **1999**, *121* (6), 1359−1364.
(14) Hirao, H. The Effects of Protein Environment and Dispersion on the Formation of Ferric-Superoxide Species in myo-Inositol Oxygenase (MIOX): A Combined ONIOM(DFT:MM) and Energy Decomposition Analysis. *J. Phys. Chem. B* **2011**, *115* (38), 11278−11285.
(15) *Molecular Operating Environment, 2010.10*; Chemical Computing Group Inc.: Montreal, Quebec, Canada, 2010.
(16) Wang, J. M.; Cieplak, P.; Kollman, P. A. How Well Does A Restrained Electrostatic Potential (RESP) Model Perform In Calculating Conformational Energies Of Organic And Biological Molecules? *J. Comput. Chem.* **2000**, *21* (12), 1049−1074.
(17) Frisch, M. J.; Trucks, G. W.; Schlegel, H. B.; Scuseria, G. E.; Robb, M. A.; Cheeseman, J. R.; Scalmani, G.; Barone, V.; Mennucci, B.; Petersson, G. A.; Nakatsuji, H.; Caricato, M.; Li, X.; Hratchian, H. P.; Izmaylov, A. F.; Bloino, J.; Zheng, G.; Sonnenberg, J. L.; Hada, M.; Ehara, M.; Toyota, K.; Fukuda, R.; Hasegawa, J.; Ishida, M.; Nakajima, T.; Honda, Y.; Kitao, O.; Nakai, H.; Vreven, T.; Montgomery, J. A., Jr.; Peralta, J. E.; Ogliaro, F.; Bearpark, M.; Heyd, J. J.; Brothers, E.; Kudin, K. N.; Staroverov, V. N.; Keith, T.; Kobayashi, R.; Normand, J.; Raghavachari, K.; Rendell, A.; Burant, J. C.; Iyengar, S. S.; Tomasi, J.; Cossi, M.; Rega, N.; Millam, J. M.; Klene, M.; Knox, J. E.; Cross, J. B.; Bakken, V.; Adamo, C.; Jaramillo, J.; Gomperts, R.; Stratmann, R. E.; Yazyev, O.; Austin, A. J.; Cammi, R.; Pomelli, C.; Ochterski, J. W.; Martin, R. L.; Morokuma, K.; Zakrzewski, V. G.; Voth, G. A.; Salvador, P.; Dannenberg, J. J.; Dapprich, S.; Daniels, A. D.; Farkas, O.; Foresman, J. B.; Ortiz, J. V.; Cioslowski, J.; Fox, D. J. *Gaussian 09*, Revision B.01; Gaussian Inc.: Wallingford, CT, 2010.
(18) (a) Siegbahn, P. E. M.; Himo, F. Recent Developments Of The Quantum Chemical Cluster Approach For Modeling Enzyme Reactions. *J. Biol. Inorg. Chem.* **2009**, *14* (5), 643−651. (b) Himo, F. Quantum Chemical Modeling Of Enzyme Active Sites And Reaction Mechanisms. *Theor. Chem. Acc.* **2006**, *116* (1−3), 232−240.
(19) (a) Becke, A. D. A Mixing of Hartree-Fock and Local Density-Functional Theories. *J. Chem. Phys.* **1993**, *98*, 1372. (b) Becke, A. D. Density-Functional Thermochemistry 0.3. The Role of Exact Exchange. *J. Chem. Phys.* **1993**, *98* (7), 5648−5652. (c) Handy, N. C.; Cohen, A. J. Left-Right Correlation Energy. *Mol. Phys.* **2001**, *99* (5), 403−412. (d) Lee, C. T.; Yang, W. T.; Parr, R. G. Development Of The Colle-Salvetti Correlation-Energy Formula Into A Functional Of The Electron-Density. *Phys. Rev. B* **1988**, *37* (2), 785−789. (e) Stephens, P. J.; Devlin, F. J.; Chabalowski, C. F.; Frisch, M. J. Ab-Initio Calculation Of Vibrational Absorption And Circular-Dichroism Spectra Using Density-Functional Force-Fields. *J. Phys. Chem.* **1994**, *98* (45), 11623−11627. (f) Vosko, S. H.; Wilk, L.; Nusair, M. Accurate Spin-Dependent Electron Liquid Correlation Energies For Local Spin-Density Calculations − A Critical Analysis. *Can. J. Phys.* **1980**, *58* (8), 1200−1211.
(20) Chen, H.; Hirao, H.; Derat, E.; Schlichting, I.; Shaik, S. Quantum Mechanical/Molecular Mechanical Study on the Mechanisms of Compound I Formation in the Catalytic Cycle of Chloroperoxidase: An Overview on Heme Enzymes. *J. Phys. Chem. B* **2008**, *112* (31), 9490−9500.
(21) (a) Alfonso-Prieto, M.; Vidossich, P.; Rovira, C. The Reaction Mechanisms Of Heme Catalases: An Atomistic View By Ab Initio Molecular Dynamics. *Arch. Biochem. Biophys.* **2012**, *525* (2), 121−130. (b) Vidossich, P.; Alfonso-Prieto, M.; Rovira, C. Catalases Versus Peroxidases: DFT Investigation Of H_2O_2 Oxidation In Models Systems And Implications For Heme Protein Engineering. *J. Inorg. Biochem.* **2012**, *117* (0), 292−297. (c) de Visser, S. P. What External Perturbations Influence The Electronic Properties Of Catalase Compound I? *Inorg. Chem.* **2006**, *45* (23), 9551−9557.
(22) Lill, S. O. N. Application of Dispersion-Corrected Density Functional Theory. *J. Phys. Chem. A* **2009**, *113* (38), 10321−10326.
(23) (a) DiLabio, G. A. Accurate treatment of van der Waals Interactions Using Standard Density Functional Theory Methods With Effective Core-Type Potentials: Application To Carbon-Containing Dimers. *Chem. Phys. Lett.* **2008**, *455* (4−6), 348−353. (b) Mackie, I. D.; DiLabio, G. A. Interactions in Large, Polyaromatic Hydrocarbon Dimers: Application of Density Functional Theory with Dispersion Corrections. *J. Phys. Chem. A* **2008**, *112* (43), 10968−10976.
(24) Bushnell, E. A. C.; Gauld, J. W. An Assessment Of Pure, Hybrid, Meta, And Hybrid-Meta GGA Density Functional Theory Methods For Open-Shell Systems: The Case Of The Nonheme Iron Enzyme 8R−LOX. *J. Comput. Chem.* **2013**, *34* (2), 141−148.
(25) Reiher, M.; Salomon, O.; Hess, B. A. Reparameterization Of Hybrid Functionals Based On Energy Differences Of States Of Different Multiplicity. *Theor. Chem. Acc.* **2001**, *107* (1), 48−55.
(26) (a) Cances, E.; Mennucci, B.; Tomasi, J. A New Integral Equation Formalism For The Polarizable Continuum Model: Theoretical Background And Applications To Isotropic And Anisotropic Dielectrics. *J. Chem. Phys.* **1997**, *107* (8), 3032−3041. (b) Mennucci, B.; Cances, E.; Tomasi, J. Evaluation Of Solvent Effects In Isotropic And Anisotropic Dielectrics And In Ionic Solutions With A Unified Integral Equation Method: Theoretical Bases, Computational Implementation, And Numerical Applications. *J. Phys. Chem. B* **1997**, *101* (49), 10506−10517. (c) Mennucci, B.; Tomasi, J. Continuum Solvation Models: A New Approach To The Problem Of Solute's Charge Distribution And Cavity Boundaries. *J. Chem. Phys.* **1997**, *106* (12), 5151−5158. (d) Tomasi, J.; Mennucci, B.; Cances, E. The IEF Version Of The PCM Solvation Method: An Overview Of A New Method Addressed To Study Molecular Solutes At The QM Ab Initio Level. *J. Mol. Struct.: THEOCHEM* **1999**, *464* (1−3), 211−226.
(27) (a) Zhao, Y.; Truhlar, D. G. The M06 Suite Of Density Functionals For Main Group Thermochemistry, Thermochemical Kinetics, Noncovalent Interactions, Excited States, And Transition Elements: Two New Functionals And Systematic Testing Of Four M06-Class Functionals And 12 Other Functionals. *Theor. Chem. Acc.* **2008**, *120* (1−3), 215−241. (b) Zhao, Y.; Truhlar, D. G. Density Functionals With Broad Applicability In Chemistry. *Acc. Chem. Res.* **2008**, *41* (2), 157−167.
(28) Fita, I.; Rossmann, M. G. The Active-Center Of Catalase. *J. Mol. Biol.* **1985**, *185* (1), 21−37.
(29) Ye, S.; Neese, F. Accurate Modeling of Spin-State Energetics in Spin-Crossover Systems with Modern Density Functional Theory. *Inorg. Chem.* **2010**, *49* (3), 772−774.
(30) Lundberg, M.; Morokuma, K. Protein Environment Facilitates O-2 Binding In Non-Heme Iron Enzyme. An Insight From ONIOM Calculations On Isopenicillin N Synthase (IPNS). *J. Phys. Chem. B* **2007**, *111* (31), 9380−9389.